

Concurrent Rate-Adaptive Reading With Passive RFIDs

Ge Wang^{ID}, Member, IEEE, Shouqian Shi^{ID}, Huazhe Wang^{ID}, Yi Liu, Chen Qian, Senior Member, IEEE, Cong Zhao^{ID}, Member, IEEE, Wei Xi^{ID}, Member, IEEE, Han Ding^{ID}, Member, IEEE, Zhiping Jiang^{ID}, Member, IEEE, and Jizhong Zhao, Member, IEEE

Abstract—Radio frequency identification (RFID)-assisted management systems have been widely applied in warehousing, logistics, retailing, etc. In these scenarios, RFID-aided applications, e.g., object tracking and human behavior sensing, rely on a high-efficiency tag reading to realize accurate analyses and timely responses. However, serious tag collisions in those large-scale RFID systems will inevitably lead to significant decreases in the tag reading rates. To meet the strict timeliness requirements of those practical applications, we aim to treat the individual reading rate for each item tag differently and focus more attention on those user-interactive ones. However, due to unpredictable user behaviors, it is impractical to infer the user-interactive tags in advance. In addition, keeping focusing on them for continuous monitoring despite user movements and multipath-prevalent environments is also challenging. To solve these problems, we propose Spotlight, the first concurrent rate-adaptive reading system in passive RFIDs. Spotlight screens the ID-agnostic user-interactive tags by proposing a multichannel feature for narrow-band RFID systems without any hardware or protocol modification and achieves rate-adaptive reading by implementing real-time MU-MIMO beamforming. Substantial experiments with 1000+ COTS RFID tags exhibit that Spotlight outperforms the commercial reader by 2.7x and the SDR-based reader by 6.12x. In addition, Spotlight first proposes the online parallel decoding method to realize concurrency among multiple users, which breaks the commercial protocol's throughput ceiling (37%) and achieves up to 59% throughputs.

Manuscript received 11 April 2022; revised 29 June 2022; accepted 15 August 2022. Date of publication 5 September 2022; date of current version 22 December 2022. This work was supported in part by the National Key Research and Development Program of China under Grant 2020YFB1707700; in part by NSFC under Grant 61832008, Grant 62002284, and Grant 62072367; in part by the China National Postdoctoral Program for Innovative Talents under Grant BX20200269; in part by the China Postdoctoral Science Foundation under Grant 2020M683494 and Grant 2021M692563; and in part by the Fundamental Research Funds for the Central Universities under Grant xzy012020010. The work of Shouqian Shi, Yi Liu, Chen Qian, and Huazhe Wang was supported in part by the National Science Foundation under Grant 1750704, Grant 1932447, and Grant 2114113. (Corresponding author: Cong Zhao.)

Ge Wang, Wei Xi, Han Ding, and Jizhong Zhao are with the Faculty of Electronic and Information Engineering, Xi'an Jiaotong University, Xi'an 710049, China (e-mail: wangge@xjtu.edu.cn; xiwei@xjtu.edu.cn; dinghan@xjtu.edu.cn; zjz@xjtu.edu.cn).

Shouqian Shi, Huazhe Wang, Yi Liu, and Chen Qian are with the Department of Computer Engineering, University of California at Santa Cruz, Santa Cruz, CA 95064 USA (e-mail: sshi27@ucsc.edu; huazhe.wang@ucsc.edu; yliu634@ucsc.edu; cqian12@ucsc.edu).

Cong Zhao is with the School of Mathematics and Statistics, Xi'an Jiaotong University, Xi'an 710049, China (e-mail: drzhaocong@gmail.com).

Zhiping Jiang is with the School of Computer Science and Technology, Xidian University, Xi'an 710126, China (e-mail: jiangzp.cs@gmail.com).

Digital Object Identifier 10.1109/JIOT.2022.3202843

Index Terms—Radio frequency identification (RFID), wireless communication.

I. INTRODUCTION

WITH the wide deployments in retailing, warehousing, and many other applications, the passive radio frequency identification (RFID) technique has become a promising solution toward item management [1], [2], [3], [4], [5], [6], [7], [8], [9], [10], [11], [12], object tracking [13], [14], [15], [16], [17], [18], [19], [20], human movement sensing [21], [22], [23], [24], [25], etc. In these applications, timely responses and accurate analyses mainly rely on a high reading rate of a small fraction of specified tags. We can easily find many examples of important RFID applications. As shown in Fig. 1, in a supermarket, the managers want to observe each customer's shopping behavior and discover the popular commodities. In a busy logistic warehouse, workers need to keep scanning the moving cargo for trajectory records and anomaly detection. In an RFID-assisted factory, assemblers always need continuous monitoring of the accessories in their current operating areas. In these applications, most tagged objects are stationary. Only a few items are moving or interacting with the users (e.g., the customers, workers, etc.). We call tags on these items as our *tags*. In fact, most RFID-assisted applications, such as object tracking and human behavior sensing, need timely monitoring of the target tags, not all the tags. That is because:

- 1) without sufficient replies from the target tags, we cannot capture the complete profile of moving trajectories/interacting behaviors. For instance, collecting ten replies from a specific tag among 1000 tags costs about 1.34 min even with the optimal system settings [26], which is obviously unacceptable in these applications;
- 2) stationary tags do not urgently require a high reading rate because their states remain unchanged. Therefore, we should treat the individual reading rate for each tag differently and perform a *rate-adaptive reading*, which improves the reading rates of target tags while decreasing that of the stationary tags.

To reach this goal, two typical solutions are proposed, namely, ID-based selective reading and energy redistribution. For the first one, many researchers focus on designing innovative algorithms based on the ID distributions of either the target tags or the entire tag population [27], [28], [29], [30], [31].



Fig. 1. Two typical RFID-assisted applications.

However, these approaches assume that managers know the ID information of both target tags and other tags, which cannot be satisfied in many applications. In contrast, the energy redistribution methods do not have any assumptions about the tag IDs. Its basic idea is to enhance the received power of some of the tags while decreasing others. In this way, only the tags with enough energy will reply. The reading rates of these tags increase due to the fewer tag collisions and higher signal-to-noise ratios (SNRs). Directional antennas employed in current RFID systems draw on the essence of energy redistribution. However, they do not work concurrently and have to track users by mechanical rotations, which limits their usages in multiuser applications. Hence, neither of them can be directly adopted in the aforementioned applications.

In fact, realizing rate-adaptive reading faces enormous challenges. First, it is not an easy task to screen out the target tags among billions of tags in practice. Due to the unpredictable user behaviors, target tags are always ID-agnostic and altering with time. Even worse is that the deployment environments of RFID systems are not only complex but also dynamic, which also makes the target tag screening error-prone. In addition, concurrent monitoring of multiple users is a common demand in many applications. Sequential sensing and tracking are neither efficient nor accurate. Third, minding the billions of deployed RFID tags, the rate-adaptive reading approach should conform to the commercial RFID protocol. Since the battery-free RFID tags cannot run sophisticated anti-collision algorithms, they have to follow the slotted ALOHA protocol, which is a broadcast protocol and notorious for its inefficiency and the bounded low reading rate.

To solve these problems, we propose Spotlight, the first real-time concurrent rate-adaptive reading prototype in passive RFID systems. Spotlight can improve the reading rate of these ID-agnostic target tags without any prior knowledge. To do so, we first screen out the target tags by comparing the channel similarities between each item tag with the reference tags. Then, we keep focusing on the target tags to continuously improve their reading rates during the user activities. To do so, we extract a multichannel “fingerprint” for the narrow-band passive RFIDs by sending a short-term frequency-modulated continuous wave (FMCW) frame. And to achieve sustained monitoring in dynamic environments, we implement an MU-MIMO beamforming prototype and adopt a genetic algorithm to update transmission parameters efficiently.

Our contributions are summarized as follows.

- 1) We implement an efficient MU-MIMO beamforming prototype for passive RFID systems, enabling sustained tracking on the target tags despite surrounding environments. Spotlight supports both the single-user case and multiuser case. To realize concurrent monitoring on multiple users, we propose an online parallel decoding (OPD) mechanism in COTS passive RFID systems. OPD first breaks the throughput ceiling (37%) [26] bounded by the commercial protocol and improves it to 59%.
- 2) We extract a multichannel feature for narrow-band RFID systems by designing a short-term FMCW frame. This approach is neither interfering with the routine RFID communications nor requiring any hardware or protocol modification. Experimental results show that our method can effectively screen out the target tags with just two replies from a given tag.
- 3) We design Spotlight, the first ID-agnostic concurrent rate-adaptive reading prototype in the COTS RFID system. Substantial experiments with 1000+ passive RFID tags in practical environments show that Spotlight outperforms the USRP-based SDR reader by up to 6.12× and the COTS RFID reader by up to 2.7×.

The remainder of this article is organized as follows. We introduce the related work in Section II. The design of Spotlight can be found in Sections III–V. We exhibit the experimental results in Section VII. Finally, we conclude this work in Section IX.

II. RELATED WORK

Target Tag Selective Reading: Target tag selective reading is an effective way to realize ID-based rate-adaptive reading. Current selective reading methods fall into three categories.

- 1) *ID-Selective Reading:* These works aim to find out the difference between the target tags and other tags and design appropriate ID-based filtering methods to realize selective reading. Among them, Tash [12] filtered the nontarget tags with a hash function and achieve efficient cardinality estimation and missing tag detection. Tagwatch [32] proposed an ID-based selective reading method to improve the reading rates of target tags.
- 2) *Tag Searching:* These researches [33], [34], [35], [36] aim to find target tags from a large volume of tags using bitmaps. Among them, Zheng and Li [33] utilized bitmaps to aggregate a large number of RFID tag information for target tag searching. Liu *et al.* [37] first used the testing slot technique to obtain the local search results by iteratively querying the target tags.
- 3) *Tag Polling:* Besides tag searching, a lot of researches focus on sensing information obtainment from the sensor-augmented tags [27], [29], [30], [31]. Among them, LocP [27] is an efficient localized polling protocol to collect information from a wanted subset of interrogated tags in a large-scale RFID system. Qiao *et al.* [28], [29] proposed two energy-efficient polling protocols to collect real-time information, and they conduct thorough simulations to verify the effectiveness.

In summary, the prior works mainly focus on utilizing a hash-based method to screen out the target tags, which relies on the knowledge of the tag ID information. Hence, there is no prior solution can cope with the ID-agnostic selective reading.

Beamforming With RFIDs: Benefiting from the promising ability to strengthen the transmitting power, many beamforming-based prototypes/theory models are proposed. Based on their applications, we divide them into three categories.

- 1) *Reading Range Enlargements* [7], [38], [39]: These researches aim to power up tags with a long distance. Among them, PushID [7] presented a novel blind distributed beamforming algorithm to search through the parameter space of beamforming weights to enlarge the tag reading range. BABF [38] proposed a method for channel measurements to improve the interrogation range.
- 2) *Transmission Quality Improvements* [39], [40], [41], [42]: To improve the transmission quality of power-constrained devices, many researchers adopt beamforming techniques. For example, Arnitz and Reynolds [40] proposed a power optimization method to enhance the transmission quality. Denicke *et al.* [39] proposed a MIMO RFID model for channel measurements, which can be applied in future generations of 5G RFID readers in conjunction with multiantenna tags. Kim *et al.* [41] provided a thorough exploration for SNR improvements with the MIMO-RFID system and evaluated its performance with simulations.
- 3) *Long-Range Localization* [43]: Some beamforming-based devices like Impinj xArray [43] are released to support accurate tag localization. However, these dedicated devices are much more expensive and are mainly used to find out the exact positions of some ID-specified tags.

However, the aforementioned solutions cannot be adopted in our real-time concurrent rate-adaptive reading applications. The reasons are threefold. First, timeliness is not a fateful factor in these applications and hence is rarely considered in the solutions [7], [38], [39], [40], [41], [42], [44]. They do not need to alter their transmission parameters according to the current situation and give a real-time response with low latency. Second, most of these solutions focus on ID-specified tags. For example, the localization system needs the tag ID as the input. Third, many of these methods are theory models [38], [41], which may face practical problems in the real world. To sum up, all these solutions cannot be adopted to address the real-time rate-adaptive reading problem.

III. OVERVIEW

A. Problem Specification

Spotlight aims to solve the concurrent rate-adaptive reading problem for ID-agnostic tags. Specifically, we assume that each item in the inventory area is labeled with a passive RFID tag, which is called the *item tag*. Our goal is to improve the reading rates of the *target tags* among all the item tags. The target tag is defined as the ones that are “interacting” with the

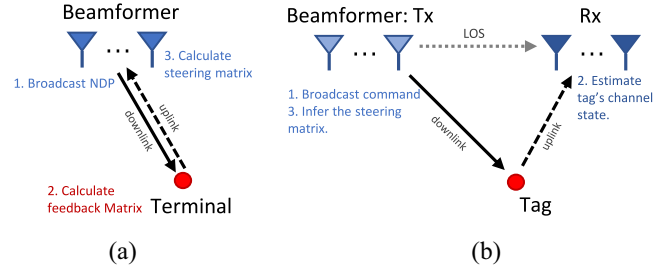


Fig. 2. Beamforming processes of Wi-Fi and RFID. (a) Beamforming in 802.11ac. (b) Beamforming with RFID systems.

users, while others are *nontarget tags*. Here, interacting means the tagged item is moving by the user or being interfered with a very close range by the user actions. For example, the accessories in the current operating areas and the commodities that are picked up by a customer can be seemed as our targets. Hence, the target tag population is altered according to the user behavior. Users have no idea about the number or locations of the target tags and nontarget tags. That makes sense because 1) most users have no RFID reader to access tagged items and 2) people cannot predict all their activities in the future. Note that we *do not* have any assumption about the ID distributions of either the target tags or the nontarget tags. We also do not assume the user movement trajectories and the inventory environment situations. To screen out the target tags among a large tag population, we employ a *reference tag* for each user. That makes sense because, in many scenarios, users always carry some routine equipment. For example, workers wear labor suits and have working cards, and customers use shopping carts to place the commodities. The reference tags can be embedded into this routine equipment and will not increase users’ burden. Note that we allow multiple users to coexist in one inventory area. We also allow complicated environmental factors, including static reflectors like furniture and walls, possible obstacles, and even moving objects.

Our basic idea is to reallocate the spatial energy by implementing RFID-based beamforming in the working area. Beamforming is a promising solution to change the spatial energy allocation in the inventory area, which can strengthen the received power of some tags while bringing down others. By dynamically adjusting the transmission settings, we can form the beams toward the target tags, and therefore increase their reading rates by improving their communication quality and reducing the collision probabilities. However, due to the characteristic of passive RFIDs, implementing beamforming faces extra difficulties, which will be detailed discussed in the next section.

B. Beamforming With RFID Systems

Before presenting the unique challenges with passive RFID systems, we first elaborate on the beamforming process in most wireless techniques. We take the beamforming design in 802.11ac as a comparison. As shown in Fig. 2(a), to obtain the steering parameters toward remote terminals, the beamformer first broadcasts a control frame called the null data packet (NDP). After receiving the NDP, each terminal returns

a feedback matrix, which provides its current channel states. With the terminals' feedback, the beamformer can finally calculate the steering matrix for the following transmission.

Obviously, mechanism above *cannot* be directly adopted in energy-constrained RFID systems. Unlike these powerful terminals like laptops or telephones, the passive RFID tag has no power supply or calculation modules. It reports data by backscattering the carrier waves sent by the beamformer. As a result, the beamformer in RFID systems should take all the tasks during the communication, including energy supply, channel state estimation, and steering matrix inference. Putting all these heavy loads on the beamformer is very challenging. First, the beamforming process is asymmetrical in RFID systems. As shown in Fig. 2(b), the beamformer has to infer the downlink channel states according to the uplink signals, which may be error-prone. In addition, considering the prevalent and time-varying multipath effects, the beamforming parameters should keep changing as well. In the following sections, we will tackle these challenges and illustrate our system design.

IV. SYSTEM DESIGN

The rate-adaptive reading problem can be divided into two subproblems, i.e., how to screen out the target tags among the large tag population and how to find out the appropriate beamforming parameters for them. For the former one, we employ a reference tag for each user and extract an irrelevant-factor-independent feature for comparison. And for the latter one, we propose a heuristic method to update the beamforming parameters in real time. More details are as follows.

A. Target Tag Screening

To improve the reading rates of the target tags, we need to screen them out first. As aforementioned, the target tags are the ones that are interacting with the users. In other words, if we can tell the state-varying tags around the user, the problem would be solved. Obviously, keep monitoring every item tag and finding out eligible ones is very time consuming and inaccurate [25], [32]. Hence, we employ a few *reference tags*, whose IDs are recorded in our system. Each user takes a reference tag along with him/her. By comparing the channel states between the reference tag and item tags, we can find out the state-varying tags around the user, say, the target tags.

However, it is not an easy task to extract accurate channel states due to the nonnegligible hardware diversity among tags and complex indoor environments. Besides, different beamforming settings may also introduce knotty variables in the comparison. To handle this problem, we propose a novel multichannel feature, which has nothing to do with the hardware diversities and beamforming settings. In the following, we will first specify the propagation model of RFID communication and then introduce our method.

1) *Irrelevant Factors Elimination*: The propagation model between the beamformer and an RFID tag is shown in Fig. 3. Specifically, a tag shows two states by turning its circular impedance, namely, "ON" and "OFF" (we use "N" and "F" for short in the following). When the switch is "N," the tag

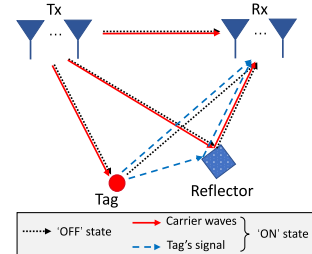


Fig. 3. Propagation model.

acts as a short terminal and modulates the incident electromagnetic waves. While when the switch is "F," the tag serves as an open terminal and reflects like an ordinary item [17]. By shifting the states between "N" and "F," a tag can send messages. According to the Friis transmission equation, the received power P_{R_i} at the receiver end R_i can be represented as follows:

$$P_{R_i} = \frac{\lambda^2 P_T G_T G_{R_i} h}{(4\pi d_{T \rightarrow R_i})^2} + \gamma \frac{\lambda^2 P_T G_T G_t^2 P_t G_{R_i} h_d^* h_u^*}{(4\pi d_{T \rightarrow t})^2 (4\pi d_{t \rightarrow R_i})^2} \quad (1)$$

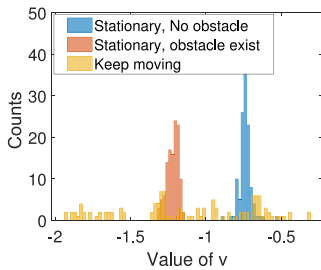
where γ equals 0 when the tag state is "F" and equals 1 when the state is "N." If we consider the transmitting antenna array as a single virtual transmitter, its transmitting power and gain are P_T and G_T , respectively. G_{R_i} and G_t are the gains of the i th receiver end and the tag. $d_{T \rightarrow R_i}$, $d_{T \rightarrow t}$, and $d_{t \rightarrow R_i}$ are the separation distances between the Tx and Rx, the Tx and the tag, and the tag and the Rx, respectively. P_t is the backscattering power of the tag, which is determined by the tag hardware characteristic and varies among different tags. h is the channel state between the Tx and Rx, which also contains environmental factors, such as reflectors and obstacles. h_d^* and h_u^* are the downlink and uplink channel states between the beamformer and the tag, respectively. Since the tag shifts its states frequently (about every 12.5 μ s), we can safely assume that the outside environment is identical for "N" and "F" states. Hence, we eliminate the common influence factors of "N" and "F" states as follows:

$$P_{R_i}(N) - P_{R_i}(F) = \frac{\lambda^2 \cdot P_T \cdot G_T \cdot G_t^2 \cdot P_t \cdot G_{R_i} \cdot h_d^* \cdot h_u^*}{(4\pi \cdot d_{T \rightarrow t})^2 (4\pi \cdot d_{t \rightarrow R_i})^2}. \quad (2)$$

According to (2), the difference between two states is also related to the beamforming parameters (i.e., transmission power P_T) and tag hardware diversities (G_t , P_t). To further eliminate these irrelevant factors, we calculate the signal division of two receiver ends and get an improved feature v , i.e.,

$$v = \sqrt{\frac{P_{R_i}(N) - P_{R_i}(F)}{P_{R_j}(N) - P_{R_j}(F)}} = \sqrt{\frac{G_{R_i} \cdot h_{ui}^*}{G_{R_j} \cdot h_{uj}^*}} \cdot \frac{d_{t \rightarrow R_j}}{d_{t \rightarrow R_i}}. \quad (3)$$

v has nothing to do with the beamforming settings and the tag diversities. It is only related to the tag position (i.e., $d_{t \rightarrow R}$) and uplink channel states (i.e., h_u^*). To evaluate the effectiveness of feature v , we try 120 beamforming settings to query one tag. The distributions of feature v are shown in Fig. 4. We find that when the tag keeps motionless, no matter whether it is shielded by some stationary obstacles, the values of v are

Fig. 4. Distributions of feature v in three cases.

very similar. Once it is moved or interfered with by users, it shows distinct variations. Hence, feature v can reflect the channel condition and motion state of an RFID tag despite the complex environments and varying beamforming settings.

2) *Multichannel Feature Extraction*: Observing the expression of feature v in (3), we find that except for the tag position, it is also vulnerable to channel fluctuations. Once the current transmitting channel is impacted by some occasional factors like frequency selective fading, the feature v may vary abruptly and fail to represent accurate information. If we can obtain a multichannel feature like the CSI in Wi-Fi, it will be more robust and reliable. However, the RFID system has a very narrow band (26 MHz). To extract a multichannel feature without any hardware or protocol modifications, we send an FMCW-based frame. Note that this approach is neither interfering with the routine RFID communications nor requiring any hardware or protocol modification. By measuring the feature v at different frequencies, we can obtain a multichannel feature vector.

Extracting an accurate feature vector from the frequency-modulated signals faces a lot of challenges. First, the FMCW-based frame will change the tag signal and make it unable to be decoded. Furthermore, the “N”/“F” states at different frequencies are also diverse, which means it is necessary to find out the corresponding “N”–“F” pair at the same frequency before doing the signal processing as (2). Hence, we send a well-designed short-term FMCW signal, which covers the first two bits of the tag preamble. According to the EPC C1G2 protocol, a tag will start with a 12-bit preamble “NNFNFFNNNN” before reporting its EPC. If we can send an FMCW frame, which just falls into the first double “N” states (marked with an underline), we can obtain $P_R(N)$ at multiple channels. However, a tag starts its reply at a random time point, namely, t_1 , which means the beamformer has no idea when the double “N” will appear. Fortunately, the tag will pick this start time within a 32- μ s time window, which ranges from 184 to 216 μ s (marked in a red rectangle in Fig. 5). The double N states last for about 24 μ s. If we send three consecutive 16- μ s FMCW frames from 184 μ s, we can fill the time window and ensure that there must be an entire FMCW frame falling in the double “N” states. Except $P_R(N)$, we also need the power of the “OFF” state, i.e., $P_R(F)$, in different channels. To this end, we send one more FMCW frame before the time window (marked in a blue rectangle in Fig. 5). In this way, by calculating the subtractions of the corresponding $P_R(N)$ and $P_R(F)$ at frequency $f(t)$, we can obtain a feature vector V as

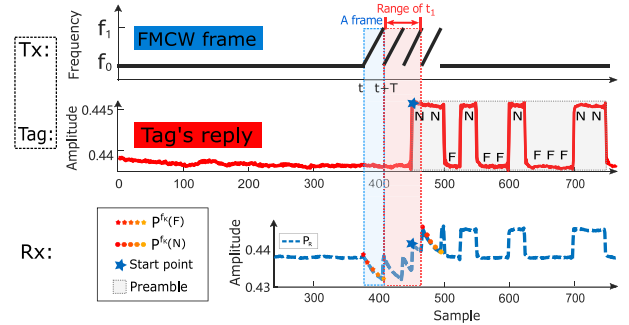


Fig. 5. Multichannel feature extraction.

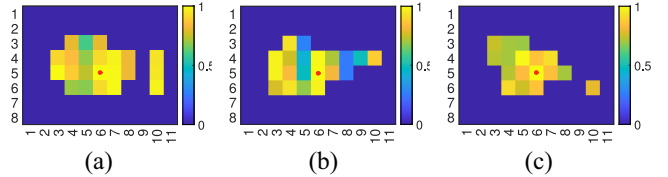


Fig. 6. Feature similarity. [The tag array has a distance of 0.45 m from the antenna array. Each cell in this figure is 8 cm \times 9 cm. The reference tag coordinates are (0, 0.45 m, 0.368 m). The dark blue cells represent the tags that do not reply. The obstacle in (b) is a 0.369 m \times 0.18 m \times 0.125 m paper box. We place it in front of the reference tag.] (a) Static environment. (b) With obstacles. (c) With interference.

follows:

$$V = [v_{f_0}, v_{f_1}, \dots, v_{f_k} \dots v_{f_n}], \text{ where } f_k = f_0 + \Delta f \cdot \Delta t_k. \quad (4)$$

In this way, we can extract a multichannel feature vector with a narrow-band RFID system. To elaborate on its effectiveness on target tag screening, we conduct an experiment and compare each tag’s feature similarity in an 8×11 tag array with the reference tag (marked in red points). The similarity is calculated with the following equation:

$$L([x, y]) = e^{-|\sum(V_{\text{ref}} - V_{[x, y]})|} \quad (5)$$

where $[x, y]$ represents the tag position. The experimental results in Fig. 6 show that even with some static obstacles or dynamic interference, tags around the reference tag show similar features. To screen out the target tags, we first treat the tags with similar features to the reference tag as candidates and then find the state-varying ones. Both the two screening steps employ experimental thresholds.

3) *Antenna Synchronizations*: Transmitting an accurate FMCW signal relies on precise frequency modulation. To eliminate the frequency and phase offsets among antennas, we adopt a prior wireless synchronization scheme presented in work MegaMIMO [45]. Specifically, node 1 is set as the master and others are slaves. We let each node send a synchronization signal one by one and compensate the phase offset to synchronize with the master node. The whole process is very time efficient and only lasts for 9.6 ms.

B. Real-Time Tracking

In the prior section, we propose a target-tag screening method. However, if we even do not receive any replies from

the target tags, the prior solution does not work. Unfortunately, we have no idea about either the IDs or the positions of target tags. Scanning all the item tags one by one is not efficient nor accurate. In this article, we propose a quick-start method before the rate-adaptive reading. The quick-start approach can help us to find out a valid beamforming steering orientation efficiently. In addition, with the time-varying environments and unpredictable user movements, the beamforming parameters should be updated timely according to the current situation. We solve this problem by introducing a heuristic method. More details can be found as follows.

1) *Quick-Start Phase*: To get rid of the aimlessly searching of target tags, we decide to find out the beamforming parameter of the reference tag instead. Since the target tags are always adjacent to the reference tag, a good parameter for the reference tag may also perform well for the target tags. Keep this in mind, we first try a series of beamforming parameters and observe which settings will result in high-energy replies from the reference tags. To do this, we keep the Tx 1 unchanged and alter the initial phase of other transmitters in the range of $[0, 2\pi)$ with a step of δ , i.e.,

$$\theta'_{T_s}(\tau) = \tau \cdot \delta + \theta_{T_s} + \Delta\theta(t), \quad \tau \in [1, 2, 3, \dots, 2\pi/\delta] \quad (6)$$

where τ denotes the index of the inventory round and ranges from 1 to $2\pi/\delta$, and we experimentally set δ as 0.2π . θ_{T_s} is the original initial phase of the slave node. We synchronize the slave with the master node by adding the phase and frequency offset $\Delta\theta(t)$. To evaluate the replies of the reference tag, we propose an energy function $E_0(\cdot)$, which are defined as follows:

$$E_0 = \sum_{i=1}^M (P_{R_i}(N) - P_{R_i}(F)) \quad (7)$$

where M is the number of receiver ends. We use a list F_0 to record the values when we tried different beamforming parameters, which is defined as follows:

$$F_0(\tau) = E_0(T_r, \Theta(\tau), \Psi(\tau)). \quad (8)$$

We call the list F_0 as the initial snapshot, which is the energy measurement of the reference tag T_r when we set the beamforming parameters as $\Theta(\tau)$ (phase) and $\Psi(\tau)$ (amplitudes), respectively. Here, we set the amplitude as the maximum value. Note that due to the prevalent multipath effects, a good beamforming setting is not only related to the tag position but also relevant to the current wireless channel.

Note that once the outside environment changes during our snapshot capture, e.g., the user walks to another position or moving objects block the line-of-sight propagation path, the snapshot will become not accurate nor reliable. To query the reference tag as efficiently as possible, we adopt the ID-specified selective reading mechanism in the current EPC C1G2 protocol. Specifically, the reader sends two commands, namely, the *SELECT* command and the *Query* command, which can be simplified as two tuples S and Q as follows:

$$S(m), Q(q) \quad (9)$$

where m is the mask code. The tuple S refers to the tags having the same ID prefixes with the mask m joining the

following inventory. q is the slot number parameter, which informs the selected tags that the slot number in the following inventory is 2^q . If we want to query the reference tag alone, the *SELECT* and *Query* commands should be set to $S(EPC)$ and $Q(0)$, respectively. Here, “EPC” is the electronic product code of the reference tag. Since only the reference tag has the same mask as the *SELECT* command, there is only one tag, i.e., the reference tag, that will take part in the following inventory. It first backscatters a 16-bit random number (RN16). After receiving a valid acknowledgment *ACK* sent by the reader, the tag will report its EPC. Note that the random number “RN16” keeps changing and is unknowable in advance. In contrast, the tag EPC is identical during communications.

To further speed up the snapshot capture process, we propose a simplified protocol called short-slot-scheme (SSS). The main idea of SSS is to skip the acknowledgment part to speed up the quick-start phase. Since we use “SELECT” command to mute all the other tags, there is only one tag, namely, the reference tag, joining the quick-start phase. Hence, we do not need to wait for the EPC replies from the reference tag. After receiving a valid RN16, it must belong to the reference tag. Note that SSS conforms to the commercial protocol and does not need any hardware modification. SSS makes the quick-start phase more efficient. It only costs 34 ms and decreases the running time by about 64.85% compared with the commercial protocol.

2) *Real-Time Parameter Updates*: By capturing an initial snapshot, we can glance at the channel states of the reference tag. However, our goal is to improve the reading rates of the target tags. To do so, we need to update the beamforming settings according to the current situations of target tags in real time. In this part, we adopt a genetic algorithm to update the beamforming parameters in a heuristic way. The basic idea is simple but effective: we analyze the current snapshot to determine the following beamforming parameters. Our algorithm can be divided into parent selection, crossover, and mutation, which are specified as follows.

Parent Selection: Intuitively, an appropriate beamforming setting will result in a larger energy in the snapshot. Hence, by comparing the snapshot values, we can find out the optimal beamforming parameter in the current solution set. However, the parameter candidates in the quick-start phase are very limited, which makes the system inflexible and incompetent. To explore more effective beamforming settings, we implement a genetic algorithm in our system, i.e., generating a child solution based on the current generation. Specifically, we sort the current snapshot F_n and select the parents as the top two records. For the first inventory round, we consider the initial snapshot F_0 as the first generation. And for the following iterations, we first evaluate the fitness f_n of the current settings, i.e.,

$$f_n = (E_n^r(T_r, \Theta_{n-1}, \Psi_{n-1}))^{W_n^r} \quad (10)$$

where W_n^r evaluates the mobility of the reference tag T_r , and $E_n^r(\cdot)$ is the energy function, which is defined as

$$E_n^r(T_r, \Theta_{n-1}, \Psi_{n-1}) = E_0(T_r, \Theta_{n-1}, \Psi_{n-1}) \mu^{\sum_{t=1}^N \eta_t^{-1} - \beta N_u} \quad (11)$$

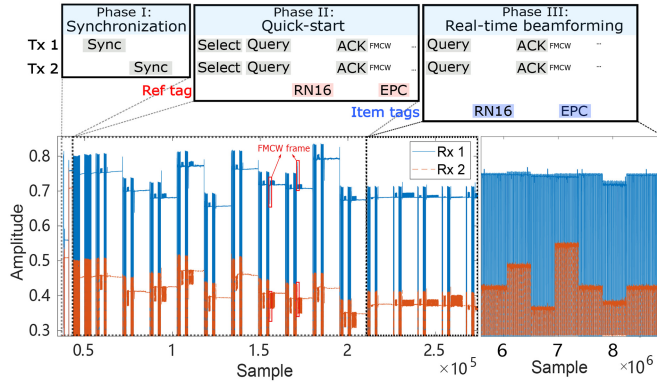


Fig. 7. Running process of Spotlight.

where n is the number of iterations, and μ is an experimental coefficient. η_t refers to the reading times of the target tag T_t in the latest inventories. N_t and N_u are the numbers of the target tags and the nontarget tags we read in this inventory round. β is an experimentally selected parameter to make $\beta \cdot N_u$ comparable to N_t . The evaluation function $E'_n(\cdot)$ considers the tag's power and the reading times of the target tags. Compared with reading a part of target tags frequently, we prefer to read more new target tags. To sum up, the snapshot F_n of the n th iteration is defined as follows:

$$F_n = \begin{cases} F_0, & n = 0 \\ C \cdot [\alpha \cdot F_{n-1}, f_n], & n > 0 \end{cases} \quad (12)$$

where α is the attenuation parameter, which is helpful to ensure the data's freshness. In addition, to cope with users' possible movements, we employ the hidden Markov model (HMM) algorithm, which estimates the user movements probability vector C by analyzing the reference tag's received signal.

Crossover and Mutation: To introduce more flexibility in the next generation, we cross and mutate the parents as follows:

$$\begin{cases} \Delta\theta_n = \varepsilon_c (\omega_f \Delta\theta_{n-1}^f + \omega_m \Delta\theta_{n-1}^m) + \varepsilon_m \mathfrak{R}_\theta \\ \psi_n(T_x) = \varepsilon_c (\omega_f \psi_{n-1}(T_x) + \omega_m \psi_{n-1}(T_x)) + \varepsilon_m \mathfrak{R}_\psi \end{cases} \quad (13)$$

where ω_f and ω_m represent the weights of the father and mother parameters, respectively. ε_c and ε_m are the crossover weight and mutation weight. \mathfrak{R}_θ and \mathfrak{R}_ψ are two random functions. In this way, Spotlight can generate a new beamforming parameter and then try it in the next iteration. Spotlight repeats the two steps in each iteration round. It is possible, although unusual, that Spotlight loses the focus on the target tags. In this case, Spotlight will restart from the quick-start phase.

C. Put All Together

We exhibit the running process of Spotlight in Fig. 7. In summary, we first synchronize each node by sending a prescribed signal one by one. Then, we obtain an initial snapshot of the reference tag in the quick-start phase. According to the initial snapshot, we start the beamforming process and update its parameters with a genetic algorithm in phase III. Note that our algorithm is a heuristic method, which means the parameters determined by our genetic method may not be

the global optimum. However, it is not critical in our application. In most user-interactive scenarios, monitoring users' activities in real time is more pragmatic than waiting for a calculated global optimum.

V. MULTIUSER CASE

In the previous section, we talked about how to update the beamforming settings in the single-user case. However, when considering multiple users, Spotlight faces more challenges. First, the reference tags of different users may collide in the quick-start phase and introduce errors in the snapshot capture. In addition, the beamforming parameter selection should consider more complex situations like the user priority, performance tradeoff, etc. To solve these problems, we first propose two mechanisms for efficient communication in the quick-start phase. And then, we illustrate how to estimate the snapshot in the multiuser case with limited information. Finally, we talked about the snapshot update policy in the multiuser case.

A. Efficient Communication in the Quick-Start Phase

In the single-user case, we employ a simplified protocol called SSS in the quick-start phase, which allows the reader to skip the EPC report procedure and restart a new inventory. That is because there is only one reference tag joining in the quick-start phase. However, in the multiuser case, there are at least two reference tags. SSS cannot be directly adopted in the multiuser case. To tackle this problem, we propose two mechanisms: 1) time-sharing SSS (T-SSS) and 2) OPD, which are specified as follows.

1) *Time-Sharing Short-Slot-Scheme:* As shown in Fig. 8(a), if we implement the SSS for each reference tag, Spotlight can obtain their snapshots one by one. By combining their snapshots, we can finally get a composite snapshot for the following beamforming transmitting. T-SSS is effective and efficient but lacks concurrency, i.e., snapshots of different reference tags are captured asynchronously and may be error-prone in some dynamic cases. As shown in Fig. 8(b), if we decode collision reference tags in real time, we can obtain their snapshot concurrently. To reach this goal, we propose the OPD method.

2) *Online Parallel Decoding:* Compared with the state-of-the-art offline parallel decoding methods, the OPD allows the reader to decode tags' collision signals in real time. The offline parallel decoding methods are effective on decoding multiple collision RN16s, but they cannot generate valid ACKs in time. Therefore, current offline parallel decoding methods cannot obtain tags' EPC and hence do not improve the throughput actually [46], [47], [48], [49].

To solve this problem, we are the first to propose the OPD. OPD faces many challenges: first, the whole decoding procedure should stick to the time limits restricted by the commercial protocol. According to the EPC C1G2 protocol, a tag waits for a valid acknowledgment for 500 us at most, or it will refuse to reply with its EPC. Second, many dynamic factors (e.g., environment variations) will introduce unpredictable errors, making the decoding error-prone. As shown in Fig. 9(a)

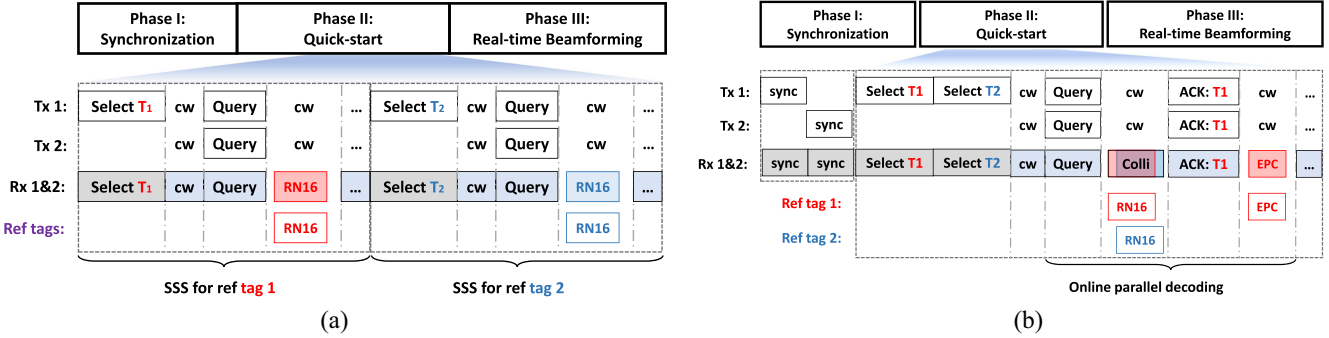


Fig. 8. Possible solutions in the multiuser case. (a) T-SSS. (b) OPD.

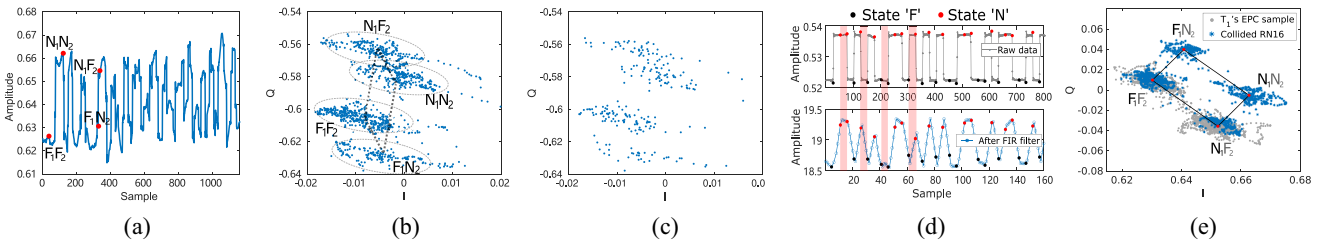


Fig. 9. Amplitudes and I - Q planes of the collision signals. (a) Collision signal's amplitude. (b) Collision signals' I - Q plane. (c) After downsampling. (d) After FIR filter. (e) Collided RN16 and EPC.

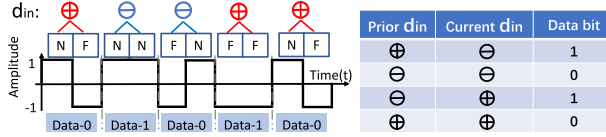


Fig. 10. Mechanism for single tag decoding.

and (b), both the amplitudes and I - Q values of collision signals are not reliable. However, even if only one bit is wrongly decoded, the communication will fail. Third, to meet the strict time requirements of the entire communication, Spotlight has to implement a downsampling toward all the received signals. However, a sufficient sampling rate is crucial to parallel decoding. The sampling rate of a typical offline parallel decoding approach [46] is 25 MHz, while the sampling rate after down-sampling in our system is only 0.8 MHz, which is $0.032\times$ of the state of the art. As shown in Fig. 9(c), the lack of samples will inevitably lead to ambiguities and misjudgments in the decoding procedure. Spotlight solves all these problems and first realizes OPD by just observing 32 samples. The experimental results in Section VII-B3 show that up to 99.1% tag collisions can be successfully decoded with OPD.

Before we elaborate on the decoding methods in OPD, we first introduce how to decode one tag. As shown in the left part of Fig. 10, the difference between the data-0 and data-1 is whether there is a state transition in the middle. Here, “N” represents the “ON” state, and “F” represents the “OFF” state of the tag. Intuitively, by comparing the values of two halves of one data bit, we can decode it easily. To do so, we pick two samples with a gap of $T/2$, where T is the length of a data bit, and compute their difference as follows:

$$d_{in} = (s_{1st} - s_{2nd}) \cdot \text{Im}(N) \quad (14)$$

d	State transition
\ominus	$N_1N_2 \rightarrow N_1N_2, N_1F_2 \rightarrow N_1N_2, F_1F_2 \rightarrow N_1N_2, F_1N_2 \rightarrow N_1N_2$
\oplus	$N_1N_2 \rightarrow F_1F_2, N_1F_2 \rightarrow F_1F_2, F_1N_2 \rightarrow F_1F_2, F_1F_2 \rightarrow F_1F_2$
\ominus/\oplus	$N_1N_2 \rightarrow F_1N_2, F_1F_2 \rightarrow N_1F_2, N_1F_2 \rightarrow F_1N_2, F_1N_2 \rightarrow N_1F_2$ $N_1N_2 \rightarrow N_1F_2, N_1F_2 \rightarrow N_1F_2, F_1N_2 \rightarrow F_1N_2, F_1F_2 \rightarrow F_1N_2$

Fig. 11. Sign of d .

where $\text{Im}(N)$ is the imaginary value of an “N” state picked in the preamble. s_{1st} and s_{2nd} represent the sample obtained from the first half and the second half of a data bit, respectively. Obviously, data-0 is very easy to tell, while data-1 is not. To get rid of ambiguities introduced by signal fluctuations, we employ an FIR filter to smooth the received signals [as shown in Fig. 9(d)]. In this way, the signs of d_{in} between the same states are also definite (i.e., $d_{in} < 0$ for $N \rightarrow N$, and $d_{in} > 0$ for $F \rightarrow F$). With the decoding mechanism shown in Fig. 10, i.e., considering both the prior d_{in} and the current one, we can correctly decode one tag.

However, if two tags’ signals collide with each other, the method mentioned above does not work. Remind that there are four states in the collision signal, namely, N_1N_2 , N_1F_2 , F_1N_2 , and F_1F_2 , where 1 and 2 represent which tag the state belongs to. In other words, 16 state transitions may happen at any possible time point. As shown in Fig. 11, not all the difference d_{in} s have definite signs. To solve this problem, we propose a method called backward inference (BI). BI has two main ideas, namely, peremptory state transition between data bits and definite relationship between d_{in} and d_{out} . Here, d_{out} represents the difference between the sample in the second half of the previous data bit and the one in the first half of the current data bit. The peremptory state transition means that each tag will change its state between each data bit with the FM0 modulation mechanism. As a result, four indefinite

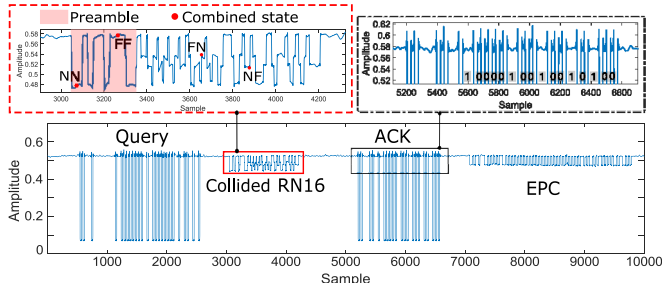


Fig. 12. Spotlight can realize OPD.

state transitions (marked in red in Fig. 11) will never happen between Tag 1's data bit. And for the remaining four indefinite state transitions, Tag 1 always changes its states, while Tag 2 may not. If we pick the tag with a larger amplitude as Tag 1, we can safely assume that the absolute value of Tag 1's d_{out} is always larger than that of Tag 2. However, only deciding the sign of d_{out} is insufficient for tag decoding. Because we decode the tag with d_{in} , not d_{out} . Fortunately, we notice that the state difference d_{in} always has an opposite sign with its next d_{out} . In other words, once we know the positive/negative of d_{out} , we can infer the sign of its prior d_{in} . In this way, we can correctly decode Tag 1 with the one-tag decoding mechanism. The example in Fig. 12 shows that Spotlight can accurately decode the collided signals and make the communication successful.

The OPD method is very efficient and takes at most 75 ms for two tags. The current OPD only supports dual tags. But by grouping every two reference tags, we can apply it in more-user cases. Except for the quick-start phase, OPD also contributes to the target tag reading.

B. Snapshot Capture in MultiUser Case

In the single-user case, we calculate the tag's power $P_R(N) - P_R(F)$ under each beamforming setting and feed them into the snapshot. This process is the same for the T-SSS. However, since there is only one tag (Tag 1) reporting its EPC in the OPD mechanism, we need to infer the corresponding power of another tag (Tag 2) from the collided RN16s. To obtain the power of Tag 2, we need to know the exact difference between F_1N_2 and F_1F_2 , or N_1N_2 and N_1F_2 . As shown in Fig. 9(e), we can distinguish the states F_1F_2 and N_1F_2 with Tag 1's EPC signal. But it is still difficult to distinguish the remained states correctly and efficiently. We address this problem by utilizing the collided preamble. As aforementioned, the range of t_1 is about 32 μ s. And the first two "N" states in the preamble last for about 24 μ s. Hence, even if the two tags start to reply at different time points, their two N states still collide with each other (24μ s + 24 μ s > 32 μ s). We pick the middle sample in the collided double "N"s, it must be the state N_1N_2 . With states N_1N_2 and N_1F_2 , we can infer the received power of Tag 2 by calculating $|N_1N_2 - N_1F_2|$. With the snapshot of each reference tag, we update the combined snapshot F_n by multiplying all of them. We also consider each user's mobility by altering the weight W_n^r of the corresponding reference tag. We give higher priority to the active users and decrease the weights of static ones.

Algorithm 1: CoA Algorithm

Input: The number of the idle/collision slot $\mathcal{S}_e/\mathcal{S}_c$

Output: The slot number parameter q

Initial: $q = \lfloor \log_2 \sqrt{2} \mathcal{N}_i - 1 \rfloor$, where \mathcal{N}_i is an initial estimation of the tag quantity.

Calculate the theoretical values of the idle/collision slot ($\mathcal{T}_e/\mathcal{T}_c$) when the total tag number is 2^q .

Set a threshold \hbar .

while Current slot $\mathcal{F}_i < \hbar \cdot \mathcal{F}$ **do**

 | Record the number of \mathcal{S}_e and \mathcal{S}_c ; \mathcal{F}_i++ ;

end

if $\mathcal{S}_e > \mathcal{T}_e$ **then**

 | $q--$; Send Quary adjust with q;

else if $\mathcal{S}_c > \mathcal{T}_c$ **then**

 | $q++$; Send Quary adjust with q;

else

 | Keep q unchanged.

end

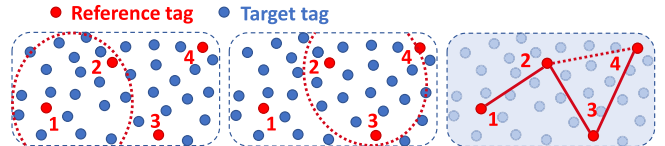


Fig. 13. Multireference tags can be modeled as a graph.

VI. FURTHER IMPROVEMENTS

In the real-time beamforming phase, choosing an appropriate slot number q is also important for performance improvements. A smaller q will result in severe tag collisions, while a larger q will lead to slot wastes. It is well known that when the slot number, say \mathcal{F} , equals the tags' quantity, say \mathcal{N} , the throughput expectation reaches the peak, i.e., 0.37. In our system, we realize OPD, which allows the reader to decode one tag even if the collision happens. The optimal slot number reduces to $(\sqrt{2}/2)\mathcal{N}$, and the reading process speeds up by 1.4 \times (due to the page limits, we skip the theoretical details). In addition, the maximum communication throughput increases from 0.37 (e^{-1}) to 0.59 ($(1 + \sqrt{2})e^{-\sqrt{2}}$).

The optimal slot number varies with the total number of tags that fall in our reading areas. To maintain a good throughput, we propose an algorithm called Compare and Adjust (CoA) to choose the slot number dynamically (as shown in Algorithm 1). The basic idea of CoA is to compare the current collision/idle slot number with the theoretical ones and then increase or decrease the slot number accordingly.

Adaptive Reading Area: In some cases, users want to scan a larger reading region. Under this circumstance, we can employ multiple reference tags for one reading area. In the experiments, we find that when the beams focus on one of the reference tags, they may also cover adjacent reference tags. As shown in Fig. 13, we can model these reference tags as a connected graph to traverse this reading area. We can model these reference tags as a connected graph to traverse this reading area. Scanning all the reference tags is a graph traversal problem. We restart the quick-start phase if none of the other reference tags can be found.

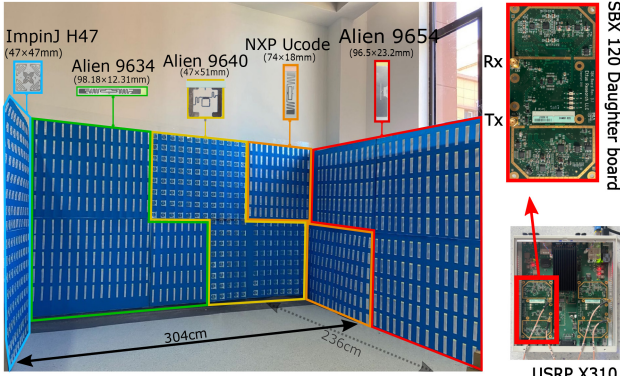


Fig. 14. System setup of Spotlight.

To prevent our system from reading unrelated reference tags, we propose a “Select, Write, and Select” method. Specifically, we set different marks in *USER* memory for each tag, say \mathcal{M} for item tags and \mathcal{R} for reference tags. We mute the unrelated reference tags by setting twice *select* and once *write*

$$S(\text{EPC}, \text{ID}, 0), W(\text{USER}, \mathcal{M}), S(\text{USER}, \mathcal{M}, 0). \quad (15)$$

This way, only the item, and user-related reference tags will reply and join the inventory.

VII. IMPLEMENTATION AND EVALUATION

A. Methodology

System Setup: As shown in Fig. 14, we implement Spotlight on a testbed of USRP X310 software-defined radios with two SBX daughter boards operating as the RFID reader. We employ four omnidirectional antennas with a gain of 12 dBi. The USRP is connected to a 64-bit GIGABYTE desktop via a PCIe cable. The desktop runs Ubuntu 16.04 and is equipped with an i9-10900 CPU. We use 1036 commercial passive RFID tags in five types, including 224 ImpinJ H47, 212 Alien 9634, 200 Alien 9640, 200 NXP Ucode 7, and 200 Alien 9654. Among them, 1000 tags are nontarget tags. Others are reference tags and target tags. For each user, we employ one reference tag and 14 target tags. Note that we just used 14 target tags in our experiments. Spotlight can support more target tags with any irregular grid layout. The separation distances between each tag are 7~14.5 cm.

Baseline: We compare Spotlight against two competing schemes.

- 1) *Commercial-Off-the-Shelf RFID Reader (COTS for Short):* We use an ImpinJ R420 reader for comparison. The modulation mode is “FM0,” and the transmitting power is 25 dBm.
- 2) *USRP-Based Software-Defined Reader (USRP for Short):* We use the recently developed USRP Gen 2 [50] reader with identical settings with Spotlight. We employ the same omnidirectional antennas for fairness.

Metric: We use the *reading rate* as the metric in our evaluation, which equals the reading times per second.

Multiple Scenarios: We evaluate the performance of Spotlight in four different cases.

- 1) *Moving Arbitrarily:* In this case, each user takes a reference tag and 11 target tags along with him/her. The user keeps walking arbitrarily inside the working area.
- 2) *Being Interfered:* In this case, both the reference tags and target tags are motionless. Meanwhile, we ask a volunteer to wave his hand arbitrarily in front of them.
- 3) *Moving in a Crowded Environment:* (We use “Blockage” for short). We place a 0.84 m × 0.44 m × 0.34 m paper box between the antennas and the tag array. Other settings are the same as the first scenario.
- 4) *Moving in a Multipath-Prevalent Environment:* (We use “Multipath” for short). In this scenario, except for the users, we also ask 1 to 2 volunteers to play as the irrelevant walkers to introduce dynamic influences.

We conduct experiments of these four cases in both the single-user case and the multiuser case.

B. Experiment Results

1) *Single-User Case:* We first evaluate the performance of Spotlight when there is only one user inside the inventory area. As shown in Fig. 15, except for the target tags, we also exhibit the reading rates of the nontarget tags for comparison. We find that Spotlight outperforms both the USRP-based reader and COTS reader and improves the reading rates of target tags by 3.63× and 1.93× on average in these four cases. If there are obstacles inside the working area, Spotlight increases the target tag reading rates by 2.7×.

To evaluate the performance of Spotlight on coping with dynamic multipath effects, we conduct an experiment and ask one or two volunteers to play as the irrelevant walkers. As shown in Fig. 15(d), we find that with severe time-varying multipath effects, Spotlight can achieve a good reading rate (9.6 #/s), which outperforms the COTS reader by 1.37×.

2) *Multiuser Case:* We also evaluate the performance of Spotlight when there are multiple users coexist. As shown in Fig. 16, we evaluate the performance of Spotlight when there are two users. We employ “T-SSS” and “OPD” in the quick-start phase. The results show that both the two algorithms can achieve high reading rates, outperform the USRP-based reader by 5.23× and 6.12×, and outperform the COTS reader by 1.22× and 1.43×. Even with three users, Spotlight outperforms USRP-based reader and COTS reader by 5× and 1.83× on average (as shown in Fig. 17). Here, we employ T-SSS in the quick-start phase.

3) *Other Factors (Synchronization Accuracy):* Note that the two daughter boards on USRP X310 are not self-synchronized [52]. To evaluate the performance of Spotlight on synchronization, we conduct a set of experiments to observe the phase offsets with or without synchronization processing. As shown in Fig. 18(a), we measure the phase offsets after a given time duration, which ranges from 28 ms to 1.792 s. The result shows that without the phase synchronization processing, the phase offset after 224 ms will be larger than 0.01 in rad. And it can be up to 0.025 ($\approx 0.004\pi$) after about 1.8 s, which will introduce fewer or more errors in transmitting beamforming signals. On the contrary, without synchronization processing, the phase offset is always smaller than 0.002

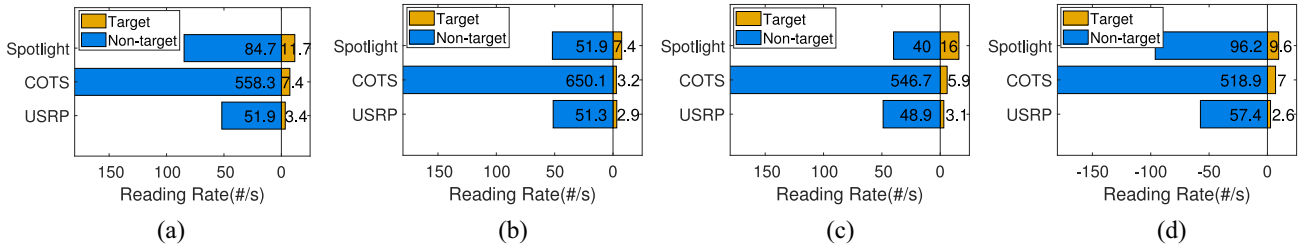


Fig. 15. Reading rates of the single-user case under different scenarios. (a) Moving arbitrarily. (b) Being interfered. (c) Blockage. (d) Multipath: 1 User, 1 Walker.

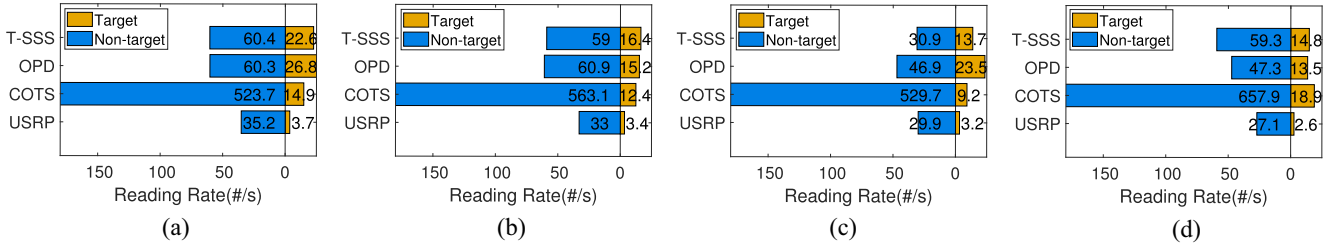


Fig. 16. Reading rates of two-user-case under different scenarios. (a) Moving arbitrarily. (b) Being interfered. (c) Blockage. (d) Multipath: 2 User, 1 Walker.

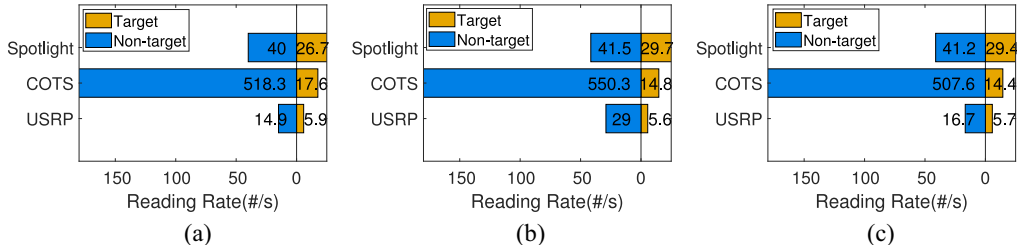


Fig. 17. Reading rates of 3-user case under different scenarios. (a) Moving arbitrarily. (b) Being interfered. (c) Blockage.

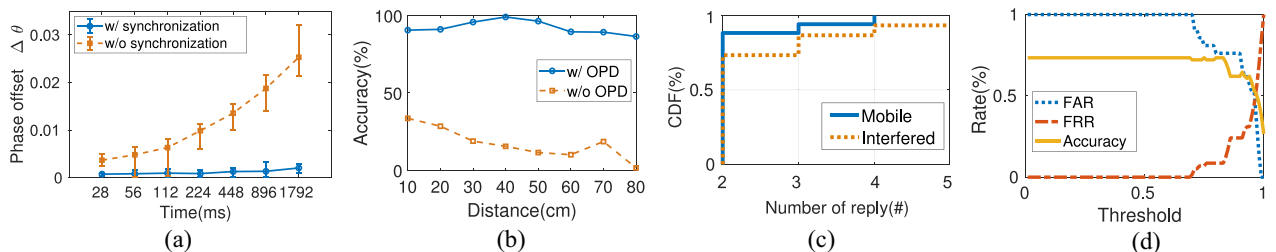


Fig. 18. Performance of Spotlight in other aspects. (a) Synchronization performance. (b) OPD accuracy. (c) State-varying detection. (d) Target tag screening.

in rad. When the time duration is smaller than 224 ms, the phase offset is smaller than 0.0009 ($\approx 0.00015\pi$). The results show that Spotlight can successfully cope with the phase and frequency offsets of distributed transmitters. And Spotlight achieves up to 12× improvements in signal synchronization.

Online Parallel Decoding Accuracy: The OPD accuracy determines the practicability of our system. In this experiment, we let two tags reply in the same slots and vary the separation distances between the reader and the tags from 0.1 to 0.8 m. At each distance, we send 2000 times single-slot inventories. The results in Fig. 18(b) show that the OPD always keeps a high accuracy (86% to 99.1%), which is much higher than the baseline (17.29%). Hence our OPD algorithm is very effective and practical.

TABLE I
DECODING COMPARISON

Method	Basic idea	Experiment	Decoding rate
[51]	BER-optimal detection	Simulation	~ 60%
RFGo [3]	Probabilistic Model	Experiment	8% ~ 75%
Ours(OPD)	Backward inference	Experiment	86% ~ 99.1%

We also compare our OPD approach with state-of-the-art online decoding methods in Table I. The comparison shows that our method outperforms other methods by 17% [3] to 32% [51].

Target Tag Screening Accuracy: The performance of Spotlight relies on an accurate target tag screening. To evaluate the performance of target tag screening methods, we first

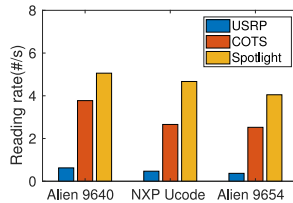


Fig. 19. Reading rate of three tag types.

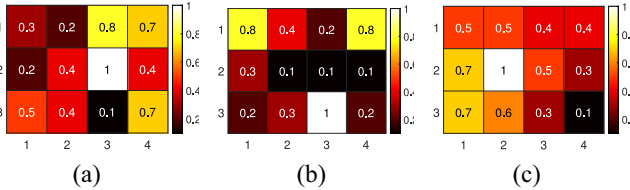


Fig. 20. Target tag reading probability when trying different reference tag placements. (a) Reference tag: (3, 2). (b) Reference tag: (3, 3). (c) Reference tag: (2, 2).

assess the sensitivity of our interaction detection. As shown in Fig. 18(c), we exhibit the CDF curve of how many replies we need to detect a state-varying tag. The results show that more than 88.24%/73.33% of state-varying tags can be detected with only two replies. We also exhibit the false accept rate (FAR) and false reject rate (FRR) of the target tag screening method. As shown in Fig. 18(d), when the threshold is 0.82, the accuracy will reach the peak, i.e., 73.42%.

Different Tag Types: We also evaluate the performance of Spotlight when we employ different types of tags as the target tags. The results are elaborated in Fig. 19. The reading rates of three different types of tags are very similar, and Spotlight outperforms the USRP-based reader and the COTS reader by 9.39 \times and 1.54 \times , respectively. Hence, Spotlight can be easily adopted in deployed RFID systems.

Separation Distances Between Reference Tag and Target Tags: To explore the influences of separation distances, we place 11 target tags around with a reference tag (marked in white) as shown in Fig. 20. Each cell is 9 cm \times 10 cm and contains one tag. The color in the cell represents the reading probability of each target tag. According to the result, we have two observations: 1) in most cases, the larger the separation distance, the lower the reading probability of the target tag and 2) the reading probability has no linear relationship with the distance increases. There may be two reasons. First, the reading probability is also related to tags' harvesting abilities. Second, the spatial energy distribution is uneven with beamforming mechanisms.

VIII. LIMITATIONS AND DISCUSSION

OPD for Multiple Users: The current OPD method only supports dual-tag online decoding, which is insufficient in large-amount tags. However, we can apply the OPD in more-user cases by grouping every two reference tags. Our future work is refining our OPD method to concurrently decode more tags in practical environments.

Limitations of OPD: The basic idea of OPD is to infer the signal of the tag with a higher amplitude. Hence, if the amplitudes of the two tags are similar, it may lead to decoding failures. However, based on our observations, many factors like tag diversities and outside environments may introduce sufficient amplitude differences for parallel decoding. Hence, our method has a good decoding accuracy in actual experiments.

Beamforming Extending: This article employs a 2 \times 2 MIMO prototype to realize beamforming in RFID. It can also be easily extended to more inputs and outputs to handle highly complex scenarios, which will be considered in our future work.

Multiuser Problems: The more the users, the lower SNR of each user. There are two possible solutions. First, increasing the number of antennas. A larger antenna array is helpful to increase the SNR of each user. Second, working in a time-sharing way. We can separate users into multiple groups and support different groups in different time slices. We will try to cope with this problem in our future work.

IX. CONCLUSION

In this article, we propose Spotlight, the first concurrent rate-adaptive reading system with COTS passive RFIDs. We resolve several practical problems and implement a prototype of Spotlight using software-defined radios. The experiments in complicated environments show that Spotlight can significantly improve the reading rate of the target tags and outperform both the USRP-based SDR reader and the COTS reader by 6.12 \times and 2.7 \times , respectively.

REFERENCES

- [1] J. Li *et al.*, "RF-rhythm: Secure and usable two-factor RFID authentication," in *Proc. IEEE Conf. Comput. Commun.*, 2020, pp. 2194–2203.
- [2] C. Zhao *et al.*, "RF-Mehndi: A fingertip profiled RF identifier," in *Proc. IEEE INFOCOM Conf. Comput. Commun.*, 2019, pp. 1513–1521.
- [3] C. Bocanegra, M. A. Khojastepour, M. Y. Arslan, E. Chai, S. Rangarajan, and K. R. Chowdhury, "RFGo: A seamless self-checkout system for apparel stores using RFID," in *Proc. ACM MobiCom*, 2020, pp. 1–14.
- [4] H. Jin, J. Wang, Z. Yang, S. Kumar, and J. Hong, "WiSh: Towards a wireless shape-aware world using passive RFIDs," in *Proc. ACM MobiSys*, 2018, pp. 428–441.
- [5] X. Chen, J. Liu, X. Wang, H. Liu, D. Jiang, and L. Chen, "Eingerprint: Robust energy-related fingerprinting for passive RFID tags," in *Proc. USENIX NSDI*, 2020, pp. 1101–1113.
- [6] U. Ha, J. Leng, A. Khaddaj, and F. Adib, "Food and liquid sensing in practical environments using RFIDs," in *Proc. USENIX NSDI*, 2020, pp. 1083–1100.
- [7] J. Wang, J. Zhang, R. Saha, H. Jin, and S. Kumar, "Pushing the range limits of commercial passive RFIDs," in *Proc. USENIX NSDI*, 2019, pp. 301–316.
- [8] G. Wang *et al.*, "Towards replay-resilient RFID authentication," in *Proc. ACM MobiCom*, 2018, pp. 385–399.
- [9] Z. An, Q. Lin, and L. Yang, "Cross-frequency communication: Near-field identification of UHF RFIDs with WiFi!" in *Proc. ACM MobiCom*, 2018, pp. 623–638.
- [10] A. Dhekne, M. Gowda, Y. Zhao, H. Hassanieh, and R. R. Choudhury, "LiquidID: A wireless liquid IDentifier," in *Proc. 16th Annu. Int. Conf.*, 2018, pp. 442–454.
- [11] J. Liu, M. Chen, S. Chen, Q. Pan, and L. J. Chen, "Tag-compass: Determining the spatial direction of an object with small dimensions," in *Proc. IEEE INFOCOM*, 2017, pp. 1–9.
- [12] L. Yang, Q. Lin, C. Duan, and Z. An, "Analog on-tag hashing: Towards selective reading as hash primitives in Gen2 RFID systems," in *Proc. ACM MobiCom*, 2017, pp. 301–314.
- [13] J. Wang and D. Katabi, "Dude, where's my card?: RFID positioning that works with multipath and non-line of sight," in *Proc. ACM SIGCOMM*, 2013, pp. 51–62.

- [14] T. Liu, L. Yang, Q. Lin, Y. Guo, and Y. Liu, "Anchor-free backscatter positioning for RFID tags with high accuracy," in *Proc. IEEE INFOCOM*, 2014, pp. 379–387.
- [15] H. Ding *et al.*, "Trio: Utilizing tag interference for refined localization of passive RFID," in *Proc. IEEE INFOCOM*, 2018, pp. 828–836.
- [16] Y. Ma, X. Hui, and E. C. Kan, "3D real-time indoor localization via broadband nonlinear backscatter in passive devices with centimeter precision," in *Proc. ACM MobiCom*, 2016, pp. 216–229.
- [17] Y. Ma, N. Selby, and F. Adib, "Minding the billions: Ultra-wideband localization for deployed RFID tags," in *Proc. ACM MobiCom*, 2017, pp. 248–260.
- [18] Y. Ma, N. Selby, and F. Adib, "Drone relays for battery-free networks," in *Proc. ACM SIGCOMM*, 2017, pp. 335–347.
- [19] T. Wei and X. Zhang, "Gyro in the air: Tracking 3D orientation of batteryless Internet-of-Things," in *Proc. ACM MobiCom*, 2016, pp. 55–68.
- [20] L. Yang, Y. Chen, X.-Y. Li, C. Xiao, M. Li, and Y. Liu, "Tagoram: Real-time tracking of mobile RFID tags to high precision using COTS devices," in *Proc. ACM MOBICOM*, 2014, pp. 237–248.
- [21] Y. Wang and Y. Zheng, "TagBreathe: Monitor breathing with commodity RFID systems," *IEEE Trans. Mobile Comput.*, vol. 19, no. 4, pp. 969–981, Apr. 2020.
- [22] H. Li, C. Ye, and A. P. Sample, "IDSense: A human object interaction detection system based on passive UHF RFID," in *Proc. ACM CHI*, 2015, pp. 2555–2564.
- [23] J. Wang, D. Vasisht, and D. Katabi, "RF-IDraw: Virtual touch screen in the air using RF signals," in *Proc. ACM SIGCOMM*, 2014, pp. 235–246.
- [24] S. Pradhan, E. Chai, K. Sundaresan, L. Qiu, M. A. Khojastepour, and S. Rangarajan, "RIO: A pervasive RFID-based touch gesture interface," in *Proc. ACM MobiCom*, 2017, pp. 261–274.
- [25] L. Shangguan, Z. Zhou, and K. Jamieson, "Enabling gesture-based interactions with objects," in *Proc. ACM MobiSys*, 2017, pp. 239–251.
- [26] L. Yang *et al.*, "Revisting tag collision problem in RFID systems," in *Proc. ICPP*, 2010, pp. 178–187.
- [27] B. Li, Y. He, W. Liu, L. Wang, and H. Wang, "LocP: An efficient localized polling protocol for large-scale RFID systems," in *Proc. IEE ICNP*, 2016, pp. 1–10.
- [28] Y. Qiao, S. Chen, T. Li, and S. Chen, "Tag-ordering polling protocols in RFID systems," *IEEE/ACM Trans. Netw.*, vol. 24, no. 3, pp. 1548–1561, Jun. 2016.
- [29] Y. Qiao, S. Chen, T. Li, and S. Chen, "Energy-efficient polling protocols in RFID systems," in *Proc. ACM MobiHoc*, 2011, p. 25.
- [30] H. Yue, C. Zhang, M. Pan, Y. Fang, and S. Chen, "A time-efficient information collection protocol for large-scale RFID systems," in *Proc. IEEE INFOCOM*, 2012, pp. 2158–2166.
- [31] H. Yue, C. Zhang, M. Pan, Y. Fang, and S. Chen, "Unknown-target information collection in sensor-enabled RFID systems," *IEEE/ACM Trans. Netw.*, vol. 22, no. 4, pp. 1164–1175, Aug. 2014.
- [32] Q. Lin, L. Yang, H. Jia, C. Duan, and Y. Liu, "Revisiting reading rate with mobility: Rate-adaptive reading in COTS RFID systems," in *Proc. ACM CoNEXT*, 2017, pp. 199–211.
- [33] Y. Zheng and M. Li, "Fast tag searching protocol for large-scale RFID systems," *IEEE/ACM Trans. Netw.*, vol. 21, no. 3, pp. 924–934, Jun. 2013.
- [34] X. Liu, B. Xiao, S. Zhang, K. Bu, and A. Chan, "STEP: A time-efficient tag searching protocol in large RFID systems," *IEEE Trans. Comput.*, vol. 64, no. 11, pp. 3265–3277, Nov. 2015.
- [35] M. Chen, W. Luo, Z. Mo, S. Chen, and Y. Fang, "An efficient tag search protocol in large-scale RFID systems," in *Proc. IEEE INFOCOM*, 2013, pp. 899–907.
- [36] S. Zhang, X. Liu, J. Wang, J. Cao, and G. Min, "Energy-efficient active tag searching in large scale RFID systems," *Inf. Sci.*, vol. 317, pp. 143–156, Oct. 2015.
- [37] J. Liu, B. Xiao, S. Chen, F. Zhu, and L. Chen, "Fast RFID grouping protocols," in *Proc. IEEE INFOCOM*, 2015, pp. 1948–1956.
- [38] S. Chen, S. Zhong, S. Yang, and X. Wang, "A multiantenna RFID reader with blind adaptive beamforming," *IEEE Internet Things J.*, vol. 3, no. 6, pp. 986–996, Dec. 2016.
- [39] E. Denicke, M. Henning, H. Rabe, and B. Geck, "The application of multiport theory for MIMO RFID backscatter channel measurements," in *Proc. Eur. Microw. Conf.*, 2012, pp. 522–525.
- [40] D. Arntz and M. S. Reynolds, "Multitransmitter wireless power transfer optimization for backscatter RFID transponders," *IEEE Antennas Wireless Propag. Lett.*, vol. 12, pp. 849–852, 2013.
- [41] D.-Y. Kim, H.-S. Jo, H. Yoon, C. Mun, B.-J. Jang, and J.-G. Yook, "Reverse-link interrogation range of a UHF MIMO-RFID system in Nakagami- m fading channels," *IEEE Trans. Ind. Electron.*, vol. 57, no. 4, pp. 1468–1477, Apr. 2010.
- [42] M. S. Abouzeid, F. Zheng, J. Gutiérrez, T. Kaiser, and R. Kraemer, "A novel beamforming algorithm for massive MIMO chipless RFID systems," in *Proc. Wireless Telecommun. Symp.*, 2017, pp. 1–6.
- [43] "ImpinJ xArray." [Online]. Available: https://rfid.atlasrfidstore.com/hubfs/Tech_Spec_Sheets/Impinj/ATLAS_Impinj_xArray_Gateway_RFID_Reader.pdf
- [44] P. Shah, "Experimental feasibility study of a passive radio frequency identification-based distributed beamforming framework and radio frequency tag design for achieving dynamic beamforming," Dept. Elect. Eng., Missouri Univ. Sci. Technol., Rolla, MO, USA, 2012.
- [45] H. S. Rahul, S. Kumar, and D. Katabi, "JMB: Scaling wireless capacity with user demands," in *Proc. ACM SIGCOMM*, 2012, pp. 235–246.
- [46] P. Hu, P. Zhang, and D. Ganesan, "Laissez-faire: Fully asymmetric backscatter communication," in *Proc. ACM SIGCOMM*, 2015, pp. 255–267.
- [47] M. Jin, Y. He, X. Meng, Y. Zheng, D. Fang, and X. Chen, "FlipTracer: Practical parallel decoding for backscatter communication," *IEEE/ACM Trans. Netw.*, vol. 27, no. 1, pp. 330–343, Feb. 2019.
- [48] J. Ou, M. Li, and Y. Zheng, "Come and be served: Parallel decoding for COTS RFID tags," in *Proc. ACM MobiCom*, 2015, pp. 500–511.
- [49] M. Jin, Y. He, X. Meng, D. Fang, and X. Chen, "Parallel backscatter in the wild: When burstiness and randomness play with you," in *Proc. ACM MobiCom*, 2018, pp. 471–485.
- [50] L. Shangguan. "USRP Gen2 reader." Accessed: Mar. 3, 2016. [Online]. Available: <https://github.com/shangdlk/Gem2-UHF-RFID-Reader/>
- [51] A. Bletsas, J. Kimionis, A. G. Dimitriou, and G. N. Karystinos, "Single-antenna coherent detection of collided FMO RFID signals," *IEEE Trans. Commun.*, vol. 60, no. 3, pp. 756–766, Mar. 2012.
- [52] "USRP X3x0." Accessed: Jul. 13, 2022. [Online]. Available: <https://kb.ettus.com/X300/X310>